JACS
JOURNAL OF THE AMERICAN CHEMICAL SOCIETY
pubs.acs.org/JACS
Article

Nonaqueous Contact-Electro-Chemistry via Triboelectric Charge

Jiajin Liu,[▽] Zhe Yang,[▽] Shaoxin Li,[▽] Yan Du, Zhiwei Zhang, Jiajia Shao, Morten Willatzen, Zhong Lin Wang,* and Di Wei*

Cite This: J. Am. Chem. Soc. 2024, 146, 31574−31584
Read Online
ACCESS | Metrics & More | Article Recommendations | Supporting Information

ABSTRACT: Mechanochemistry revolutionizes traditional reactions through mechanical stimulation, but its reaction efficiency is limited. Recent advancements in utilizing triboelectric charge from liquid−solid contact electrification (CE) have demonstrated significant potential in improving the reaction efficiency. However, its efficacy remains constrained by interfacial electrical double-layer screening in aqueous solutions. This study pioneered chemistry in nonaqueous systems via CE for catalysis and luminescence. Density functional theory simulations and experiments revealed varying electron transfer capabilities and chemoselectivity of CE across different solvents. Phenol degradation via CE in dimethyl sulfoxide (DMSO) exhibited a rate over 40 times faster than that of traditional mechano-driven chemistry. A more intuitive comparison revealed that CE degradation of phenol in DMSO exhibits a 30-fold rate improvement compared to deionized water, where the degradation remains incomplete. Luminol oxidation by radicals generated solely via CE in DMSO eliminates the dependence on traditional catalysts and side reactions, establishing a pure and simple system for investigating the reaction mechanisms. A high and stable luminescence characteristic was maintained for 3 months, enhancing the imaging accuracy and stability exponentially. This study underscores the impact of triboelectric charge on reaction efficiency and chemoselectivity, establishing a new paradigm in nonmetal catalysis, mechanoluminescence, and providing profound insights into reaction kinetics.

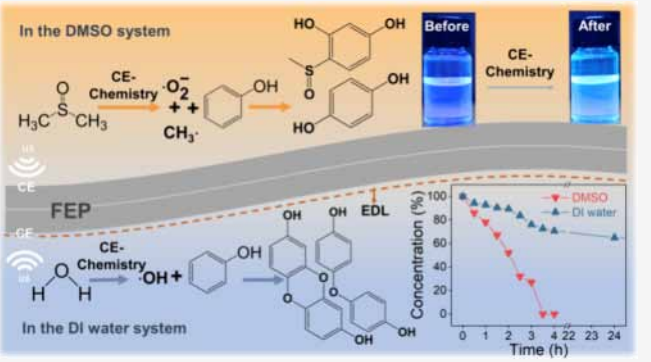

INTRODUCTION

Mechanochemistry, an interdisciplinary field, was recognized as one of the ten changing world technologies by the International Union of Pure and Applied Chemistry (IUPAC) in 2019. It not only makes known chemistry "greener" but also reveals novel reaction pathways that surpass conventional chemical methods.[1] For instance, mechanical force facilitates the selective cleavage of chemical bonds at a localized level, leading to the formation of stereoisomers and regioisomers that are otherwise unattainable under solvothermal conditions.[2] Furthermore, liquid-assisted mechanochemistry enables the direct utilization of poorly soluble sulfates, oxides, or carbonates as reactants to synthesize metal−organic materials.[3,4] This approach reduces reliance on explosive or toxic metal reagents typically used in conventional solvothermal syntheses.[5] It also expands the potential for non-noble metal catalysis,[6] aiming to explore low-cost and highly stable metal-free alternatives.[7] However, the localized and nonuniform nature of extreme mechanochemical conditions,[8] including compression,[9] shear,[10] impact,[11] and extension,[12,13] imposes limitations on reaction efficiency. Sonochemistry is a subset of mechanochemistry that utilizes ultrasound to create cavitation and vibration effects in solutions.[14] Through these mechanical forces, polymer chains are selectively broken down, effectively converting mechanical energy into chemical processes.[15] Piezoelectric materials present a promising solution by enhancing mechanical reaction efficiency through the generation of a surface electric field based on the separation of internal piezoelectric polarization charge under stress.[16,17] Piezochemistry, based on the piezoelectric effect, finds extensive application in atom transfer radical cyclization,[18] trifluoromethylation reactions,[19] arylation and borylation reactions,[20] etc., providing mild and effective mechanical reaction conditions. However, the commonly used piezoelectric materials, such as barium titanate and lead zirconate titanate,[21] are brittle,[22] environmentally hazardous[23] due to elements like lead, and challenging to recycle. Moreover, the electron and hole, as a result of the piezoelectric effect, easily recombine once the external force is removed, thereby limiting the reaction efficiency.[24]

In contrast, triboelectric charge generated by the contact electrification (CE) effect, involving electron transfer[25,26] to form a stable surface electric field,[27] shows significant promise

Received: July 9, 2024
Revised: October 22, 2024
Accepted: October 23, 2024
Published: November 11, 2024

for enhancing reaction processes.[28] Moreover, upon contact between two surfaces, the interface-induced triboelectric charges facilitated by the CE effect typically exceed the internally induced piezoelectric polarization charge generated by the piezoelectric effect.[29] More importantly, triboelectric materials offer a wide range of choices and exhibit stable mechanical properties.[30] Accordingly, the CE effect has received extensive attention and has been employed as a contact-electro-catalysis (CEC) method to degrade methyl orange,[31,32] synthesize low-cost hydrogen peroxide,[33] and even recycle metallic materials from discarded lithium-ion batteries sustainably.[34] Recently, our preliminary research has expanded the application of CEC to encompass various chemical reactions, including redox reactions, polymerization, and fluorescence.[35] Besides, guidance that unified the concept of work functions, electronegativity in triboelectric series, and standard electrode potentials was developed based on the electron transfer capabilities, introducing the concept of contact-electro-chemistry (CE-Chemistry). In CE-Chemistry, electron transfer at the liquid−solid (L−S)[36] interface may lead to the generation of reactive radicals, initiating chemical reactions.[37] It is well-known that the CE-Chemical reactions can be induced by various solid dielectrics, such as fluorinated ethylene propylene (FEP) and polytetrafluoroethylene (PTFE). However, the reaction solvent is typically constrained to aqueous solutions, which readily form electrical double layers (EDLs), hindering the L−S interfacial electron transfer and reaction efficiency.[31,33−35] In addition to aqueous solutions, nonaqueous solvents play a vital role in chemical reactions,[38] influencing reaction rates, product yield, and even reaction mechanisms. On the other hand, the potential feasibility of CE-Chemistry in nonaqueous solvents remains unexplored, along with the impact of the CE effect between solid dielectrics and organic solvents on reactions.

This study pioneers CE-Chemistry in nonaqueous environments, exemplified by catalyzed phenol and luminol luminescence, and investigates the disparity of CE-Chemistry in various solvents (both aqueous and nonaqueous) on the L−S interfacial electron transfer. For example, the CE of FEP-deionized (DI) water exhibited challenges in completely degrading a phenol concentration of 1 mM, achieving only 40% degradation efficiency after 46 h. In contrast, the CE of FEP-dimethyl sulfoxide (DMSO) degraded the same concentration of phenol completely within 4 h. The phenol degradation rate in FEP-DMSO was over 30 times greater than that in FEP-DI water, with both systems achieving approximately 40% degradation of phenol. This advancement may stem from the fact that DMSO, as a nonaqueous solvent, does not readily form an EDL-like DI water,[39] which generates a significant amount of hydronium ions (H_3O^+) during the CE of FEP-DI water. Furthermore, the higher zeta potential of FEP observed in the FEP-DI water system indicated a denser and more stable EDL formation. It should be noted that not all organic solvents, such as *N*,*N*-dimethylformamide (DMF), will accelerate the CE-Chemical reactions. Further simulation calculations and experimental measurements proved that the inherent electron transfer capability might be the key factor regulating the CE-Chemical reaction efficiency. More importantly, the tunability of the chemical reaction was realized by CE-Chemistry in various solvents. Phenol was primarily degraded into hydroquinone, facilitated by hydroxyl ($\cdot OH$) radicals and superoxide ($\cdot O_2^-$) radicals generated in the CE of FEP-DI water. Additionally, $(C_6H_3)SOCH_3(OH)_2$ and $(C_6H_4)SOCH_3OH$ were produced in the CE of FEP-DMSO due to the methyl ($CH_3\cdot$) and $\cdot O_2^-$ radicals. This characteristic provided a robust foundation for tuning the reaction pathways and achieving the desired end product. Besides, the controllability of radicals in CE-Chemistry facilitated the study of the luminol luminescence reaction mechanism. Specifically, the luminol dianion ($LUM^{=}$) was steadily observed in the CE of FEP-DMSO. This CE-induced luminol reaction obviated the need for oxidants, such as hydrogen peroxide[40] or oxidative enzymes,[41,42] and minimized side reactions typical in a traditional approach. This advancement enhanced the potential of CE-Chemistry for long-term monitoring or sensing in luminescence applications. This study advanced the understanding of solvent effects on the L−S CE mechanism and CE-Chemical reactions, opening avenues to realize nontraditional, efficient, and controllable chemical reactions through the CE physical process. CE-Chemistry enables the regulation of electron transfer between solid dielectrics and liquid to facilitate interface-confined chemical reactions, mimicking biological signal transduction (such as the synthesis and transmission of neurotransmitters) and providing probes for reaction kinetics.

RESULTS

Design Plan. The phenomenon of CE generally occurs between two contact surfaces, such as solid−solid,[43] L−S,[44] and liquid−liquid. The CE effect can convert otherwise wasted energy from collisions, vibrations, or other mechanical actions into the direct generation of surface triboelectric charge, making it particularly important in chemical reactions. Additionally, it was reported that mechanochemistry is the key to elucidating CE fundamental properties.[45] The crucial role of electron transfer in the charge transfer mechanism of L−S CE has been documented in numerous studies, offering insights into the mechanisms of CE-Chemistry.[46] It typically involves electron transfer during CE, particularly in aqueous solutions, where electrons transfer from water molecules to solid dielectrics, resulting in the generation of $\cdot O_2^-$ and $\cdot OH$ radicals that interact with surrounding substrates. Therefore, this work aims to study the impact of different solvents on CE and elucidate their influences on chemical reactions. Density functional theory (DFT) has been very popular for calculations in physics, chemistry, and materials science to investigate the electronic structure of many-body systems, such as atoms, molecules, etc. For calculating the atomic charge distribution via DFT methodologies, the Atomic Dipole moment Corrected Hirshfeld population (ADCH) analysis tool was employed to minimize dependency on user-defined parameters or assumptions and automatically adjust electron density partitioning with physically based weights, enabling more precise attribution of electrons to specific atoms.[47] First, the electron transfer (Δq) in L−S CE and the corresponding energy barriers (ΔE) are simulated by calculating the difference between the lowest unoccupied molecular orbital (LUMO) and highest occupied molecular orbital (HOMO) for FEP-various solvents and O_2-FEP under various conditions using DFT. The detailed calculated parameters are provided in Simulation Methods of the Supporting Information. An FEP film was selected as the solid dielectric due to its exceptional electro-accepting capability.

Since CE-Chemistry was typically conducted in an ultrasonic environment, the ultrasonic effect facilitated the formation of cavitation bubbles (CBs) at the L−S interface. When CBs grew

https://doi.org/10.1021/jacs.4c09318
J. Am. Chem. Soc. 2024, 146, 31574−31584

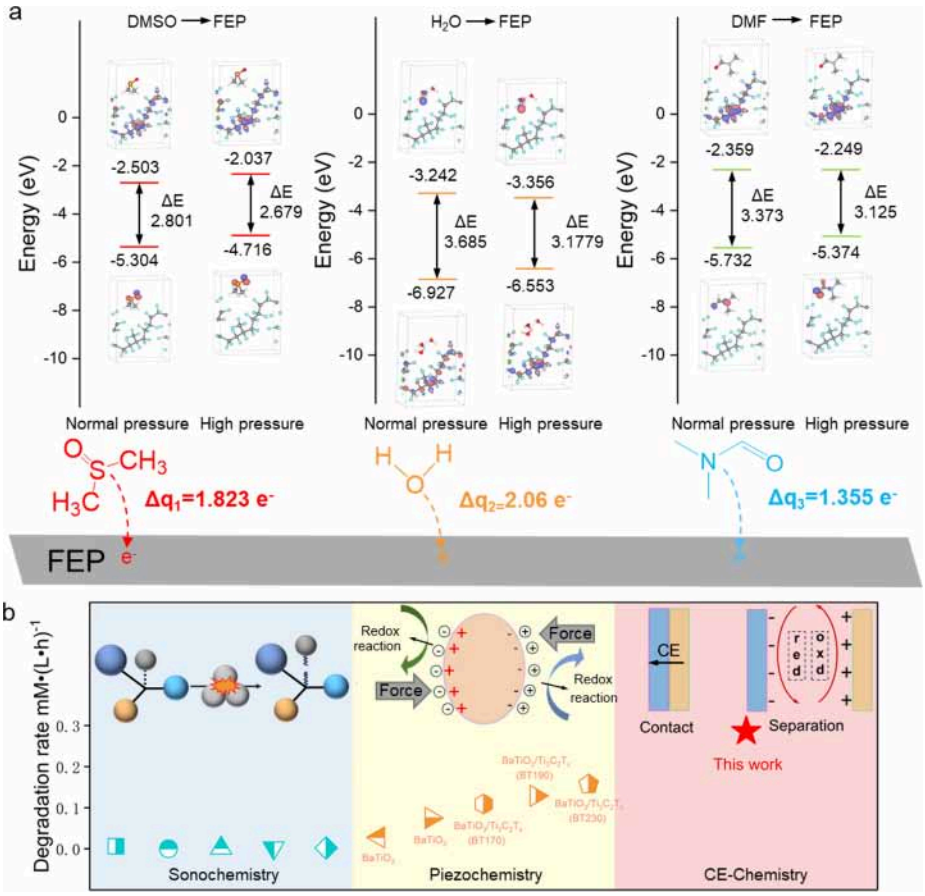

Figure 1. Theoretical simulation of electron transfer within various L−S interfaces and their CE-Chemistry. (a) DFT simulations of electron transfer energy barriers and electron transfer quantities in different solvents. (b) Comparison of phenol degradation rate with other methods and the mechanism of mechanochemistry, piezochemistry, and CE-Chemistry.

to a certain size, they burst, generating a high-pressure jet and applying pressure to the nearby L−S interface.[48] According to the transition model[25] and extensive research reports, electron transfer in CE was highly sensitive to pressure conditions. Therefore, the simulations took into account the high pressure resulting from the collapse of the CBs. Furthermore, to ensure a fair comparison of electron transfer capabilities under consistent conditions, the simulation box volume was standardized initially and finally across different FEP solvents. In the DFT simulations, high pressure was achieved by reducing the simulation box volume from 10 × 15 × 5 Å^3 (normal pressure) to 10 × 13 × 5 Å^3 (high pressure), a common method for simulating high pressure in CE-Chemistry.[31,33] Variations in electron transfer efficiency were thus attributed to differences in the solvent molecular structure. The high pressure between solvents and FEP introduced in the simulation calculations was often modeled as the CE effect. It can be observed that in the case of liquid/FEP, the calculations shown in Figure 1a revealed that the energy barrier for electron transfer decreased under high pressure. Additionally, compared to normal pressure, the theoretical values of charge transfer at the L−S interface increased, as shown in Figures S1−S3. The charge transfer (Δq) for FEP-DMSO, FEP-DI water, and FEP-DMF under high pressure increased by 14, 15.9, and 3% (Figure S4), respectively. It was noteworthy that external mechanical stimulation could reduce the ΔE and increase the Δq during CE. In addition, the calculation results showed that within the same solvent volume, the trend in the amount of electron transfer between different solvents and FEP was as follows: FEP-DI water (2.06 e$^-$) > FEP-DMSO (1.823 e$^-$) > FEP-DMF (1.355 e$^-$) (Figure 1a). The experimentally measured charge transfer amounts by an electrometer (Keithley, 6514)[49,50] were also found to be consistent with the theoretically calculated trend, namely, FEP-DMSO (1.99 nC) > FEP-DI water (1.23 nC) > FEP-DMF (1.16 nC), as shown in Figure S5. The observed differences in electron transfer could likely be attributed to the formation of the EDL at the L−S interface. According to the hybrid EDL model,[51] when water molecules lost electrons during CE, they generated H_3O^+, which then adsorbed onto the negatively charged FEP surface. This resulted in the formation of an EDL that obstructs subsequent interfacial electron transfer. The impact of the EDL on electron transfer and CE-Chemistry at the L−S interface in aqueous solutions has been demonstrated in our previous work.[35] Additionally, COMSOL simulations were conducted to analyze the potential changes during the contact separation process between FEP and various solvents (Figures S6−S8). This revealed that the FEP surface became negatively charged after CE, and the surface potential trend followed the order: FEP-DMSO > FEP-DI water > FEP-DMF, aligning with the charge transfer trend observed in the experimental measurements from the triboelectric nanogenerator. Ultrasonication stands as an efficient method within mechanochemistry, supplying high-energy power and high pressure to facilitate the environmentally friendly degradation of organic pollutants such as phenol. However, when relying solely on

https://doi.org/10.1021/jacs.4c09318
J. Am. Chem. Soc. 2024, 146, 31574−31584

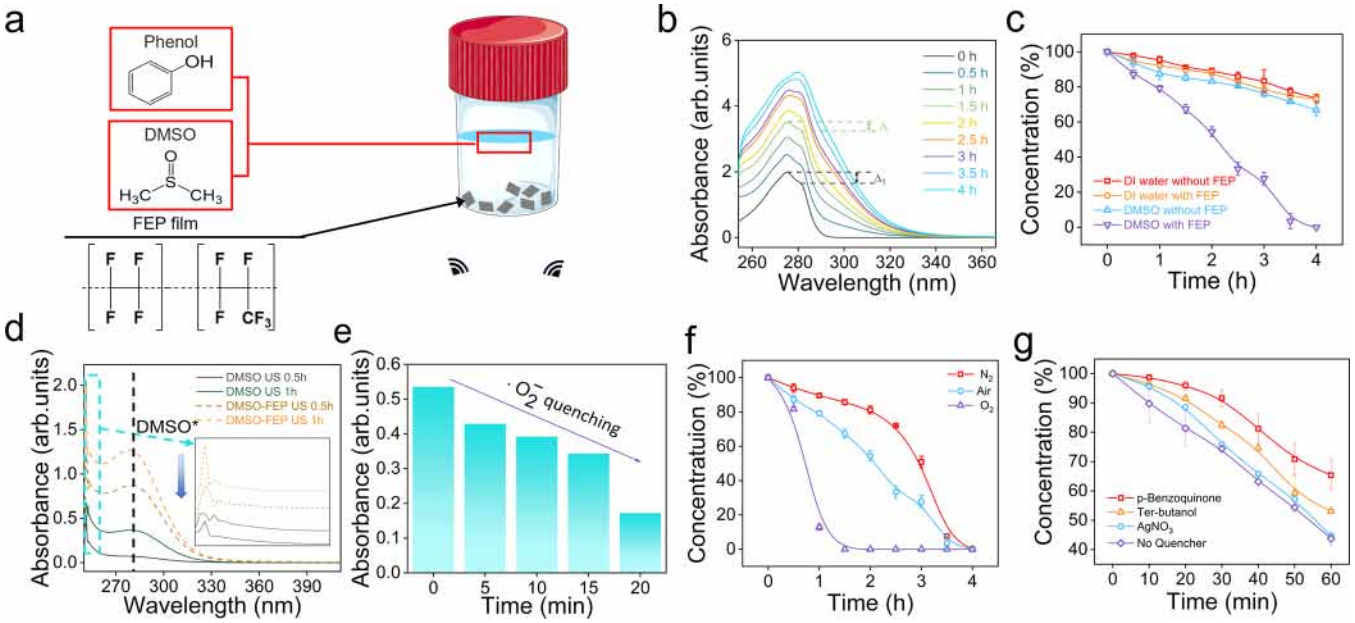

Figure 2. Study of the CE-Chemical reaction efficiency. (a) Schematic of the experimental setup and protocol. (b) UV−vis spectra of phenol during CE-Chemistry in FEP-DMSO. (c) Changes in phenol concentration during CE-Chemistry under different conditions. (d) UV−vis spectra of DMSO ultrasonicated in the presence and absence of FEP. (e) Quenching of superoxide radicals during the quiescent period. Changes in phenol concentration during CE-Chemistry in FEP-DMSO with (f) different gases and (g) different radical scavengers.

ultrasonic cavitation, the degradation rate of phenol typically ranges from 7.95×10^{-5} to 0.0064 mM/(h·L),[52−55] possibly due to nonuniform mechanical excitation. Introducing piezoelectric materials to generate polarization electric fields can effectively enhance the degradation rate to 0.028−0.157 mM/(h·L),[56−58] albeit with challenges related to limited material selection and recycling. In contrast, under ultrasonication, the degradation rate of phenol in CE of FEP-DMSO increases to 0.286 mM/(h·L), at least 40 times higher than that achieved through ultrasonication alone (Figure 1b). This enhancement can be attributed to effective contact-separation cycles induced by ultrasonication and triboelectric charge generation during CE between FEP and DMSO, promoting the degradation rate and underscoring the significant role of the CE effect in chemical reactions. Additionally, the DFT simulations were used to compare the ease of radical formation in DMSO under mechanochemistry, piezochemistry, and CE-Chemistry. In this simulation, the postbond cleavage states of DMSO within a simulation box of $10 \times 15 \times 5$ Å^3 were used as the initial state for structural optimization. The compressed box volumes necessary to sustain the ionic state, representing radical formation, are presented in Figure S9. In mechanochemistry (using sonochemistry as an example), the box volume had to be compressed to $10 \times 8 \times 5$ Å^3. In piezochemistry, with zinc oxide (ZnO) as the piezoelectric material, the box volume needed to be compressed to $10 \times 11 \times 5$ Å^3. In CE-Chemistry, with FEP as the CE material, the box volume required only minimal compression of $10 \times 13 \times 5$ Å^3. These results demonstrated that CE-Chemistry could maintain the ionic state with minimal compressed volume variation, indicating more favorable conditions or lower reaction barriers for radical generation.

Enhanced CE-Chemical Reaction Efficiency. Phenol was dissolved in DMSO to prepare the standard solution, and the concentration of phenol was precisely determined by using UV−vis spectroscopy. As illustrated in Figure S10, the discrepancy in absorbance intensity (A_{12}) at wavelengths λ_1= 272 nm and λ_2= 282 nm diminished with the decrease in the standard solution concentration, exhibiting a linear coefficient of determination (r^2) of 0.99. Consequently, the degradation efficiency of phenol (D_t) in the CE of FEP-DMSO can be evaluated by monitoring the alteration in A_{12} during the CE-Chemical process, as elucidated in the Supporting Information. The CE-Chemical experimental design for degrading phenol is illustrated in Figure 2a, where a 300×200 mm FEP film was dissected into 10×10 mm fragments and submerged in a 15 mL DMSO solvent with a concentration of 1 mM phenol. A thermostatic ultrasonication apparatus operating at a frequency of 40 kHz and a power of 500 W was utilized to enhance the CE at the interface of FEP and DMSO, leveraging the formation of CBs. As shown in Figure S11, phenol exhibited minimal degradation in the absence of vigorous mechanical stimulation from ultrasonication, with a degradation of 2.9% observed within 2 h under ultrasonic influence. Considering the potential impact of temperature on chemical reactions, a standard solution containing FEP underwent water bath heating at 20, 40, and 60 °C for 2 h. The outcomes revealed that the absorbance values of phenol's characteristic absorption peaks remained constant, indicating negligible degradation at these temperatures. However, when subjected to ultrasonication under the same temperature gradient, significant phenol degradation occurred with degradation rates escalating with temperature (Figure S12). This implied that while temperature influences the reaction rate in CE-Chemistry, the reaction is determined by the L−S CE from the solid dielectric. Additionally, the temperature of the solution was monitored during the ultrasonic process, and it was found that the reaction temperature was around 50 °C for both samples with and without FEP (Figure S13). At this temperature, no significant phenol degradation was observed in the samples heated in a water bath. This indicated that the key factor driving the reaction during the ultrasonic process is the CE

https://doi.org/10.1021/jacs.4c09318
J. Am. Chem. Soc. 2024, 146, 31574−31584

effect rather than the thermal effect of the ultrasound. As demonstrated in Figure S14, the incorporation of solid dielectrics substantially accelerated the chemical reaction. The degradation rate of phenol when FEP was in contact with DMSO was at least 3 times higher compared to the effect of cavitation alone. This phenomenon suggested that the incorporation of FEP enhanced the reaction, primarily via electron transfer during CE, as illustrated by the transition model.[25] As shown in Figure S15, atoms were attracted when beyond their equilibrium distance, but when brought closer, their electron clouds overlap, causing repulsion. This overlap facilitated electron transfer, highlighting the essential role of the potential barrier in the governing CE processes. Considering the measurement range of the experimental instruments, subsequent experiments were conducted at a temperature of 40 °C to ensure better observation while achieving faster reaction rates. Additionally, the effect of humidity on the reaction was negligible under both low (30%) and high (90%) humidity conditions, suggesting that CE-Chemical reactions predominantly occur within the bulk phase of the solution (Figure S16). To elucidate the role of CE on phenol degradation, UV−vis spectroscopy was used to measure absorbance at 30 min intervals (Figure 2b), indicating a continuous degradation of phenol. The absorbance difference between λ_1 and λ_2 decreased as time went on. As shown in Figure 2c, control experiments were conducted under the same conditions. The degradation rate of phenol in DMSO with FEP reached 100% in 4 h, whereas samples without FEP exhibited only 28% degradation within the same duration. Meanwhile, in DI water, the reaction efficiency of the samples containing FEP was also higher than those without FEP. As shown in Figure S17, the energy barriers for radical generation in DI water and DMSO were both reduced after the introduction of FEP. This indicated that the CE effect associated with FEP significantly enhances the reactions.

In addition, by comparing the reaction efficiency of phenol in DI water to that in DMSO, it was revealed that the degradation rate in DMSO was over 30 times higher than that in DI water. It can be seen from Figure S18 that phenol exhibited different UV−vis spectra in different solvents, suggesting that the solvation effect of various solvents should be considered. As shown in Table S2, although DI water has a higher dielectric constant than DMSO and DMF, theoretically facilitating electron transfer, experimental measurements indicate that charge transfer and chemical reaction efficiency in DI water are lower than those in DMSO (Figures S5 and S19). This discrepancy might be attributed to the theoretical DFT model not accounting for the effects of interfacial EDL formation. Furthermore, the formation of the EDL on FEP in various solvents was measured using the zeta potential (Figure S20). It could be observed that after ultrasonic treatment, the zeta potential of FEP in DI water (−24.93 mV) was significantly higher than that in the nonaqueous solvents DMSO (−2.79 mV) and DMF (−2.49 mV). The larger negative zeta potential value in the FEP-DI water system suggested its more stable EDL formation due to the enhanced electrostatic attraction of counterions.[59] According to the "two-step" EDL formation process of CE at the L−S interface, during the process of CE between DI water and FEP, the DI water molecules lost electrons, leading to the formation of H_3O^+ ions, which adsorbed on the negatively charged surface of FEP, rapidly forming the EDL and inhibiting subsequent electron transfer and chemical reactions. In contrast, DMSO exhibited minimal susceptibility to self-ionization and ion formation, potentially hindering the formation of an EDL that could impede chemical reaction progress. Therefore, phenol degradation in the aqueous solution nearly ceased after about 4 h (Figure S19), indicating that stable EDL formation subsequently inhibits further interfacial electron transfer, ultimately reducing the efficiency of the CE-Chemical reaction.

Despite the similar solvent properties of DMSO and DMF, it was observed that the CE-Chemical reaction rate in DMF approached zero (Figure S21). DFT simulations, encompassing the low interfacial electron transfer capability and the high potential barriers for FEP-DMF, revealed marked differences (Figures S1 and S3). Furthermore, experimental data on radical generation (Figure S20), real-time interfacial charge transfer monitoring (Figure S5), and COMSOL simulations of surface potential (Figures S6 and S8) shifts highlighted significant disparities between the FEP-DMSO and FEP-DMF systems, corroborating their divergent chemical reaction efficiencies. To investigate the root cause of these differences, we examined the electron transfer capacities of FEP-DMSO and FEP-DMF using Valence Shell Electron Pair Repulsion (VSEPR) theory,[60] molecular orbital theory,[61] and the transition model[25] (Figure S15). According to VSEPR theory and molecular orbital theory, DMF, with a dielectric constant of 36.7, has a stable structure due to its amide group and p−π conjugation,[62] which diminishes the carbonyl group's electron-donating ability. Its planar triangular arrangement of oxygen, nitrogen, and carbon atoms leads to a symmetrical electron cloud distribution, reducing electron pair repulsion.[63] In contrast, DMSO, with a dielectric constant of 46.7, features a sulfoxide group, where the sulfur atom's lone pair overlaps significantly with the oxygen atom's electrons. This increased overlap enhances mutual attraction, altering local electron density and intensifying repulsion forces.[64] Structurally, there is a significant repulsive interaction between the lone pair on the sulfur atom and the oxygen atom in the sulfur−oxygen double bond, resulting in a tetrahedral configuration. This explained the significant charge transfer observed between DMSO and FEP. These findings indicated that the intrinsic electron transfer capabilities between different solvents and solid dielectrics are critical factors in CE-Chemistry. In electrochemistry, charge transfer was fundamental, dictating both the reaction rate and direction.[65] When applied to CE-Chemistry, a sequence diagram illustrating the charge transfer capabilities and CE-Chemical reaction efficiency is shown in Figure S23. Additionally, to demonstrate the versatility of CE-Chemistry, the degradation of methyl orange (MO) was successfully achieved, as shown in Figure S24. The degradation efficiency in FEP-DMSO was significantly higher than that in FEP-DI water. Furthermore, using another mechanochemical method, ball milling, the degradation of MO was also achieved, with the degradation efficiency in FEP-DMSO surpassing that in FEP-DI water (Figure S25).

To explore the impact of FEP and DMSO on the degradation of phenol during the CE process, alterations in composition throughout CE between pure DMSO and FEP were observed by using UV−vis spectroscopy. As shown in Figure 2d, there were two absorption peaks observed at 275 and 250 nm after ultrasonication, and both peaks increased upon the addition of FEP. The peak at 275 nm corresponded to the decomposition of DMSO. It was reported that the 250 nm absorption peak corresponded to the generation of $\cdot O_2^-$ radicals, and the quenching trend of $\cdot O_2^-$ radicals with the

https://doi.org/10.1021/jacs.4c09318
J. Am. Chem. Soc. 2024, 146, 31574−31584

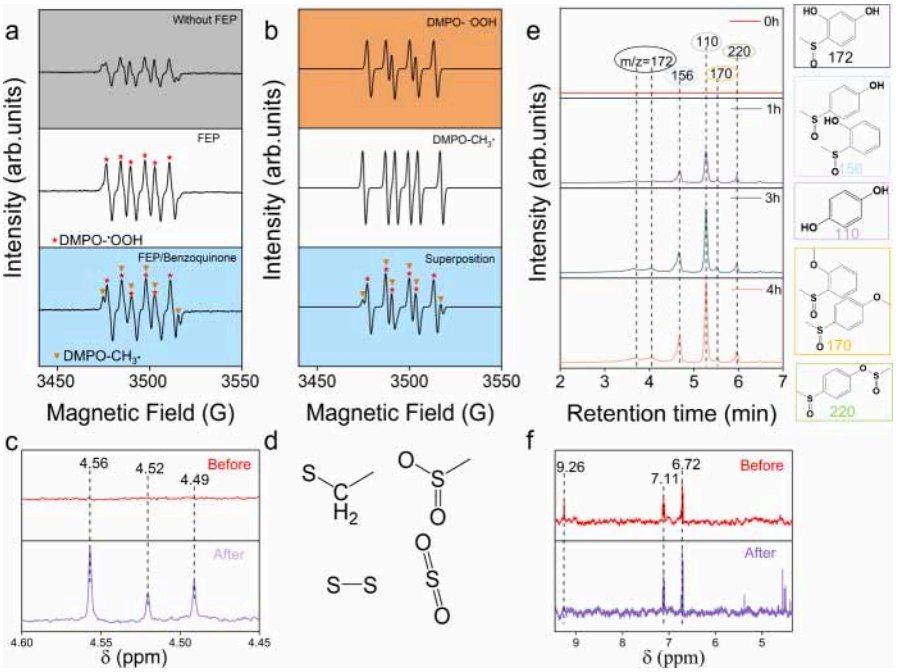

Figure 3. Analysis of the radicals generated and products met in CE-Chemistry. (a) Measured and (b) simulated EPR spectra under various conditions, and every peak was labeled by the corresponding patterns. (c) NMR patterns and (d) functional groups before and after CE-Chemical reactions in FEP-DMSO. (e) HPLC-MS and (f) NMR patterns of phenol before and after CE-Chemical reactions in FEP-DMSO.

settling time is shown in Figures 2e and S26. It was reported that the generation of $\cdot O_2^-$ radicals might be related to the presence of O_2.[66] By continuously bubbling air, N_2, or O_2 into the solution to change the concentration of O_2, the relationship between different gases and DMSO decomposition is shown in Figure S27. The peak intensity trend of DMSO decomposition and generation of $\cdot O_2^-$ radicals was O_2 > air > N_2, indicating that O_2 could facilitate the progression of the reaction (Figure S28). Similarly, in a DMSO solution of phenol (1 mM), introducing different gases yielded results, as shown in Figure 2f. The addition of O_2 facilitated phenol degradation, completing the process in 1.5 h, while N_2 addition inhibited phenol degradation, completing it in 4 h. This phenomenon aligned with the observations in pure DMSO, where O_2 enhanced the progression of the reaction. To further understand the mechanism, a series of free radical scavengers (1 mM) were added to the sample solution with 0.3 mM phenol. Tert-butanol, p-benzoquinone, and $AgNO_3$ were considered as scavengers for ·OH radicals, $\cdot O_2^-$ radicals, and electrons, respectively. The evolution of phenol concentration in the presence of these scavengers is displayed in Figure 2g. The addition of these quenchers reduced the reaction rate, indicating that both $\cdot O_2^-$ radicals and electrons play roles in the reaction. The $\cdot O_2^-$ appeared as the limiting factor as only 37.3% of phenol was degraded after 1 h when it was quenched. This underscored the pivotal roles of $\cdot O_2^-$ radicals and electrons within this system, elucidating that the regulation of $\cdot O_2^-$ radical generation can effectively influence the reaction process.

Degradation of Phenol in Nonaqueous CE-Chemistry. It has been reported that CE-Chemistry in aqueous solutions primarily depends on ·OH radicals and $\cdot O_2^-$ radicals. This paper, however, confirmed the generation of new radicals by CE in nonaqueous environments, where the $\cdot O_2^-$ and $CH_3\cdot$ radicals were detected by electron paramagnetic resonance (EPR) during CE of FEP-DMSO. Two protocols were employed: one utilizing a 100 mM 5,5-dimethyl-1-pyrroline N-oxide (DMPO) solution and the other involving a solution containing both 100 mM DMPO and 1 mM p-benzoquinone. The addition of p-benzoquinone aimed to quench $\cdot O_2^-$ radicals, thereby increasing the likelihood of $CH_3\cdot$ radicals reacting with DMPO. As shown in Figure 3a, sextuplet DMPO-·OOH characteristic peaks were observed in pure DMSO solution and were enhanced in the presence of FEP (white background), which suggested the CE-facilitated reaction. Both DMPO-·OOH (red stars) and DMPO-$CH_3\cdot$ (orange triangles) were detected after the introduction of 1 mM p-benzoquinone (blue background). Simulated EPR spectra of individual $\cdot O_2^-$ and $CH_3\cdot$ radicals, along with their superposition with respective weights of 85 and 15%, are displayed in Figure 3b. The raw code for simulation is provided in the Simulation Methods of the Supporting Information. The simulated EPR spectra aligned well with the collected data in Figure 3a, with differences attributed mainly to nonequilibrium conditions during the testing process.

Nuclear magnetic resonance (NMR) and high-performance liquid chromatography−mass spectrometry (HPLC-MS) tests were conducted to investigate the CE-Chemical reaction of FEP-DMSO with and without phenol. As shown in Figure 3c, a hydrogen peak was observed at 4.52 ppm, which was attributed to the hydrogen signal adjacent to sulfur based on its chemical shift and ^{1}H NMR splitting. Figure 3d shows the functional group structures during CE of FEP-DMSO. The HPLC-MS spectra (Figure S29) revealed the presence of seven distinct substances with mass-to-charge ratios (m/z) of 160, 188, 192, 224, 238, 246, and 252, respectively. The abundance of these substances increased as the ultrasonication time was extended. Detailed analysis of the mass spectra (Figure S30) revealed that these peaks correspond to the products of DMSO. Therefore, CE between DMSO and FEP generated $CH_3\cdot$ and $\cdot O_2^-$ radicals, which might subsequently combine to form

https://doi.org/10.1021/jacs.4c09318
J. Am. Chem. Soc. 2024, 146, 31574−31584

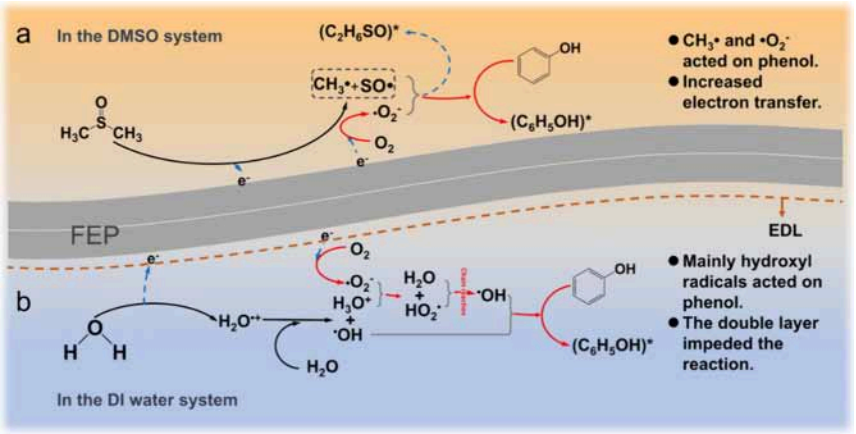

Figure 4. Mechanism of CE-Chemistry in different solvents. The mechanism of phenol degradation in CE-Chemistry of (a) FEP-DMSO and (b) FEP-DI water.

various end products. The possible reaction process in CE of FEP-DMSO might proceed as follows:

$$C_2H_6SO \rightarrow 2CH_3\cdot + SO \quad (1)$$

$$O_2\cdot + e^- \rightarrow \cdot O_2^- \quad (2)$$

$$4CH_3\cdot + 12SO\cdot + 2H_2O \rightarrow 4CH_4O_3S_3 + O_2 \quad (3)$$

$$4CH_3\cdot + 8SO\cdot + \cdot O_2^- \rightarrow 2C_2H_6O_5S_4 \quad (4)$$

$$12CH_3\cdot + 12SO\cdot + \cdot O_2^- \rightarrow 4C_3H_8O_3S_3 + 2H_2O \quad (5)$$

$$4CH_3\cdot + 16SO\cdot + \cdot O_2^- + 2H_2O \rightarrow 4CH_4O_5S_4 \quad (6)$$

$$12CH_3\cdot + 16SO\cdot + 3\cdot O_2^- \rightarrow 4C_3H_8O_5S_4 + 2H_2O \quad (7)$$

$$4CH_3\cdot + 16SO\cdot + 2H_2O \rightarrow 4CH_4O_3S_4 + 3O_2 \quad (8)$$

$$4CH_3\cdot + 8SO\cdot \rightarrow 2C_2H_6O_3S_4 + O_2 \quad (9)$$

HPLC-MS spectra (Figure 3e) showed that the products of phenol might comprise five species with m/z of 172, 156, 110, 170, and 220 after CE-Chemical reactions in FEP-DMSO. The ^{1}H NMR spectra (Figure 3f) revealed that the hydrogen signal at 9.26 ppm disappeared, indicating that phenol was completely degraded after CE-Chemistry in FEP-DMSO. Additionally, hydrogen peaks at 7.11 and 6.72 ppm were observed, which were attributed to the hydrogen signals of the benzene ring and other aromatic rings based on their chemical shifts. The reaction equations between phenol and $CH_3\cdot$ radicals, as well as $\cdot O_2^-$ radicals, were proposed as follows:

$$2C_6H_6O + \cdot O_2^- \rightarrow 2C_6H_6O_2 \quad (10)$$

$$4C_6H_6O + 4CH_3\cdot + 4SO\cdot + \cdot O_2^- \rightarrow 4C_7H_8O_2S + 2H_2O \quad (11)$$

$$2C_6H_6O + 2CH_3\cdot + 4SO\cdot + \cdot O_2^- \rightarrow 2C_7H_8O_4S_2 + 2H_2O \quad (12)$$

$$2C_6H_6O + 4CH_3\cdot + 4SO\cdot + \cdot O_2^- \rightarrow 2C_8H_{10}O_2S + 2H_2O \quad (13)$$

$$4C_6H_6O + 4CH_3\cdot + 4SO\cdot + 3\cdot O_2^- \rightarrow 4C_7H_8O_3S + 2H_2O \quad (14)$$

The CE-Chemical products of phenol in DMSO were linked to the functional groups present in DMSO, while the products in DI water were associated with hydroxyl functionalities, such as hydroquinone (Figure S31). It indicated that different solvents produce different types of radicals, leading to functional groups in the final products associated with the radicals generated by the solvent. Hence, it was demonstrated that altering solvents could tune the selectivity of the chemical reactions.

Mechanism of CE-Chemistry in Various Solvents. Figure 4a illustrates the mechanism for phenol degradation in CE-Chemistry of FEP-DMSO or FEP-DI water. During the contact between FEP and DMSO, DMSO lost electrons to generate $CH_3\cdot$ radicals and other DMSO derivatives (DMSO*), while FEP acquired electrons, forming the negatively charged state of FEP (FEP*). Simultaneously, O_2 captured electrons from FEP* to produce $\cdot O_2^-$ radicals, reverting FEP* to its initial uncharged state. Hence, the continued CE between FEP and DMSO through ultrasonication could generate numerous radicals to degrade phenol rapidly and sustainably. In contrast, CE between DI water and FEP would generate hydroxyl radical cations ($H_2O\cdot^+$) concurrently with electron transfer from water molecules to FEP (Figure 4b). Furthermore, $H_2O^{\cdot+}$ combined with DI water molecules to produce ·OH radicals and H_3O^+. Although O_2 in water captured electrons from FEP* to produce $\cdot O_2^-$ radicals, the H_3O^+ ions adsorbed onto the negatively charged surface of FEP*, forming a dense EDL. Consequently, only a limited amount of $\cdot O_2^-$ and ·OH radicals can degrade phenol in CE of FEP-DI water.

Morphological characterization and element mapping of the FEP film before and after CE-Chemistry are reported in Figure S32. No apparent changes in morphology were observed through both naked-eye examination and scanning electron microscopy. The elemental composition of multiple FEP films was analyzed before and after the reaction, revealing that the composition remained the same with only minor differences in element content (Figure S33). Furthermore, the mapping pictures indicated that the composition of the FEP remained unchanged by using energy-dispersive X-ray spectroscopy. In addition, spectroscopic analysis techniques were employed to provide more in-depth information about the chemical nature of the FEP film. Figure S34a presents Raman spectra, showing consistent skeletal vibration modes of FEP before and after the reaction. Figure S34b presents Fourier-transform infrared spectra, where the fingerprint region below 1500 cm^{-1} remains stable after the reaction with no observable changes. Figure S34c presents X-ray diffraction spectra, revealing no shift in

https://doi.org/10.1021/jacs.4c09318
J. Am. Chem. Soc. 2024, 146, 31574−31584

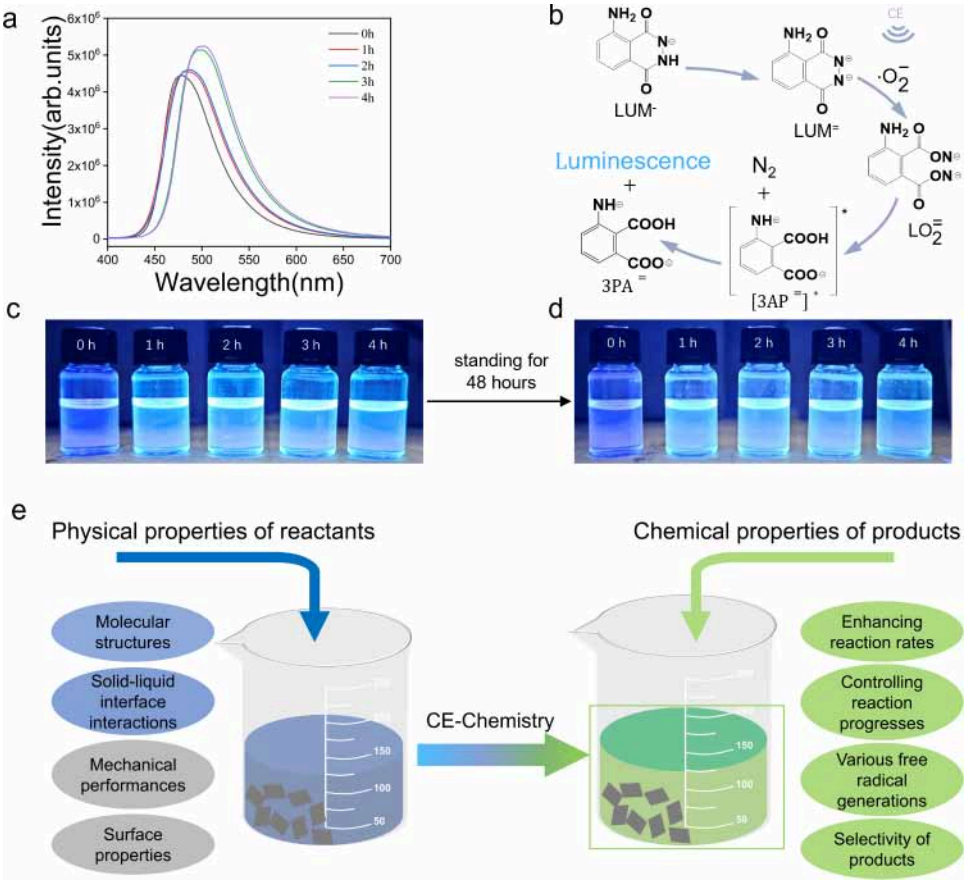

Figure 5. Broad applications of CE-Chemistry. (a) Fluorescence spectra measured at 0, 1, 2, 3, and 4 h under ultrasonication. (b) Mechanism of luminescence of luminol in DMSO. (c) Photographs of luminescence of luminol and (d) after standing in the dark for 48 h. (e) Future prospects for CE-Chemistry.

diffraction peak positions before and after the reaction. Chemical state changes in the FEP film before and after the reaction were analyzed by using X-ray photoelectron spectroscopy. The C1s, F1s, and O1s spectra of FEP are presented in Figure S35a−c, respectively. Neither a shift in binding energies of original peaks nor the generation of new peaks was observed after degrading phenol, which not only further confirmed the chemical stability of FEP during CE-Chemistry but also excluded the possibility of physical adsorption of phenol at the FEP surface. These results indicated that the pristine dielectric material FEP serves as a catalyst in the degradation of phenol.

Broad Applications of CE-Chemistry. Fluorescence analysis is widely applied for its simplicity, sensitivity, and real-time detection capabilities.[67] Fluorescent sensors, serving as a straightforward, sensitive, and nondestructive method, are extensively utilized in fields such as biological analysis and substance detection.[68] Luminol, as a classic luminescent reagent with numerous electron-rich groups, possesses excellent biocompatibility and water solubility, making it ideal for high-sensitivity fluorescence assays.[69] More importantly, luminol is a nontoxic molecule with a simple structure, easy synthesis, and low cost, leading to its widespread use, including in forensic investigations for blood detection.[70] Typically, luminol oxidation requires the addition of an oxidant or oxidative enzymes. Here, through the CE of FEP-DMSO, luminol can be oxidized without traditional oxidants, producing stable luminescence. As DMSO can stabilize free radicals[71] and the luminol dianion ($LUM^{=}$),[72] CE-Chemistry offers a unique benefit for a prolonged luminescence reaction. A 300 mm × 200 mm FEP film was introduced into a 15 mL DMSO solution containing 0.8 mM luminol and subjected to ultrasonication. Fluorescence testing successfully detected luminescence, as illustrated in Figure 5a. After allowing the reacted sample to stand in darkness for 48 h, subsequent fluorescence testing revealed no change, as depicted in Figure S36. Furthermore, significant luminescence was still observed after 3 months, as shown in Figure S37, demonstrating an enhancement in luminescence stability by orders of magnitude. The reaction equations for the luminescence of luminol in DMSO are illustrated in Figure 5b.[73] In DMSO, luminol initially forms the luminol dianion, which subsequently reacts with $\cdot O_2^-$ radicals to generate intermediate $[LO_2^-]$, ultimately producing luminescent substance $3PA^{=}$. This intermediate is subsequently transferred into the fluorescent substance $[3PA^{=}]^*$.Upon excitation, $[3PA^{=}]^*$, in which a proton from the amino group transfers to the adjacent carboxyl group, is transferred into $3PA^{=}$ to emit luminescence around 490 nm.[57] The corresponding optical images in Figure 5c,d further validated the stability of fluorescence, thereby demonstrating the application of CE-Chemistry in nonaqueous systems for investigating intermolecular interactions. Such CE-luminescence also offers the possibility to develop new biocompatible analytical methods, utilizing fluorescence-based analyses to detect and quantify specific substances in chemical reactions. Future efforts will concentrate on utilizing physical methods to regulate chemical reactions, such as surface modification of

https://doi.org/10.1021/jacs.4c09318
J. Am. Chem. Soc. 2024, 146, 31574−31584

dielectric materials and the use of diverse nonaqueous solvents, to enhance the rate of CE-Chemical reactions, generate a spectrum of radicals, and control product selectivity (Figure 5e).

CONCLUSIONS

The diverse chemical reactions facilitated by the triboelectric charge resulting from CE between FEP and various solvents highlight CE-Chemistry's efficacy and versatility in advancing the domain of mechanochemistry while also demonstrating its capability to regulate chemical reaction selectivity. A significant difference between CE-Chemistry in FEP-DMSO and FEP-DI water might stem from variations in the electron transfer capacities of solvents and the formation of interfacial EDL, reflecting differences in the ability of DMSO and DI water to lose electrons and form the EDL. Employing nonaqueous solvents to mitigate the formation of EDL represents a crucial method to overcome the constraint on reaction efficiency. The experimental results demonstrated that the CE of FEP-DI water struggled to completely degrade 1 mM phenol, achieving only 40% degradation efficiency after 46 h. In contrast, the CE of FEP-DMSO rapidly and totally degraded the same concentration of phenol within 4 h, exhibiting a degradation efficiency over 30 times higher than the former. In addition, solvents with different molecular structures generate various free radicals, resulting in the formation of products with diverse functional groups. This circumvents the limitation of solely producing two types of free radicals in aqueous systems and permits the regulation of selectivity by altering solvents. Importantly, the CE of FEP-DMSO enabled luminol oxidation without relying on traditional oxidants and side reactions and improved the luminescent effect of luminol for a period of over 3 months, enhancing its potential for various applications in long-term monitoring or sensing. This study extends the frontier of mechanochemistry and introduces an effective strategy for regulating chemical reaction selectivity, deepening our understanding of solvent effects on the L−S CE mechanism. It sets the stage for achieving nontraditional, efficient, and controllable chemical reactions through CE-Chemistry, mimicking biological signal transduction and providing insights into reaction kinetics. This advancement lays the groundwork for future endeavors aimed at achieving more precise and environmentally friendly chemical reactions.

ASSOCIATED CONTENT

Data Availability Statement

The authors declare that all the data that support the findings of this study are available within the article and Supporting Information. Source data are provided in this paper. Correspondence and requests for materials should be addressed to Z.L.W. or D.W.

Supporting Information

The Supporting Information is available free of charge at https://pubs.acs.org/doi/10.1021/jacs.4c09318.

Experimental procedures; materials; chemical reagents; sample preparation; sample characterization; simulation methods; calculation of phenol concentration; results and discussion; and references (PDF)

AUTHOR INFORMATION

Corresponding Authors

Zhong Lin Wang − *Beijing Institute of Nanoenergy and Nanosystems, Chinese Academy of Sciences, Beijing 101400, P. R. China; Beijing Key Laboratory of Micro-Nano Energy and Sensor, Center for High-Entropy Energy and Systems, Beijing Institute of Nanoenergy and Nanosystems, Chinese Academy of Sciences, Beijing 101400, P. R. China; Guangzhou Institute of Blue Energy, Guangzhou 510555, P. R. China; Georgia Institute of Technology, Atlanta, Georgia 30332-0245, United States;* orcid.org/0000-0002-5530-0380; Email: zhong.wang@mse.gatech.edu

Di Wei − *Beijing Institute of Nanoenergy and Nanosystems, Chinese Academy of Sciences, Beijing 101400, P. R. China; Centre for Photonic Devices and Sensors, University of Cambridge, Cambridge CB3 0FA, U.K.;* orcid.org/0000-0003-2670-6362; Email: dw344@cam.ac.uk

Authors

Jiajin Liu − *Beijing Institute of Nanoenergy and Nanosystems, Chinese Academy of Sciences, Beijing 101400, P. R. China; School of Nanoscience and Engineering, University of Chinese Academy of Sciences, Beijing 100049, P. R. China*

Zhe Yang − *Beijing Institute of Nanoenergy and Nanosystems, Chinese Academy of Sciences, Beijing 101400, P. R. China; School of Nanoscience and Engineering, University of Chinese Academy of Sciences, Beijing 100049, P. R. China*

Shaoxin Li − *Beijing Institute of Nanoenergy and Nanosystems, Chinese Academy of Sciences, Beijing 101400, P. R. China; School of Nanoscience and Engineering, University of Chinese Academy of Sciences, Beijing 100049, P. R. China*

Yan Du − *Beijing Institute of Nanoenergy and Nanosystems, Chinese Academy of Sciences, Beijing 101400, P. R. China; School of Nanoscience and Engineering, University of Chinese Academy of Sciences, Beijing 100049, P. R. China*

Zhiwei Zhang − *Beijing Institute of Nanoenergy and Nanosystems, Chinese Academy of Sciences, Beijing 101400, P. R. China; School of Nanoscience and Engineering, University of Chinese Academy of Sciences, Beijing 100049, P. R. China*

Jiajia Shao − *Beijing Institute of Nanoenergy and Nanosystems, Chinese Academy of Sciences, Beijing 101400, P. R. China; School of Nanoscience and Engineering, University of Chinese Academy of Sciences, Beijing 100049, P. R. China*

Morten Willatzen − *Beijing Institute of Nanoenergy and Nanosystems, Chinese Academy of Sciences, Beijing 101400, P. R. China; School of Nanoscience and Engineering, University of Chinese Academy of Sciences, Beijing 100049, P. R. China;* orcid.org/0000-0002-8215-9650

Complete contact information is available at: https://pubs.acs.org/10.1021/jacs.4c09318

Author Contributions

$^{\nabla}$J.L., Z.Y., and S.L. contributed equally.

Author Contributions

All authors have given approval to the final version of the manuscript.

Funding

This work was supported by the National Natural Science Foundation (grant number 22479016).

Notes

The authors declare no competing financial interest.

REFERENCES

(1) Do, J.-L.; Friščić, T. Mechanochemistry: A Force of Synthesis. *ACS Cent. Sci.* **2017**, *3* (1), 13−19.

(2) Zholdassov, Y. S.; Yuan, L.; Garcia, S. R.; Kwok, R. W.; Boscoboinik, A.; Valles, D. J.; Marianski, M.; Martini, A.; Carpick, R. W.; Braunschweig, A. B. Acceleration of Diels-Alder reactions by mechanical distortion. *Science* **2023**, *380* (6649), 1053−1058.

(3) Adams, C. J.; Kurawa, M. A.; Lusi, M.; Orpen, A. G. Solid state synthesis of coordination compounds from basic metal salts. *CrystEngComm* **2008**, *10* (12), 1790−1795.

(4) Friščić, T.; Fábián, L. Mechanochemical conversion of a metal oxide into coordination polymers and porous frameworks using liquid-assisted grinding (LAG). *CrystEngComm* **2009**, *11* (5), 743−745.

(5) Czaja, A.; Leung, E.; Trukhan, N.; Müller, U. Industrial MOF Synthesis. In *Metal-Organic Frameworks*; Wiley, 2011; pp. 337−352.

(6) Yu, F.; Zhou, H.; Huang, Y.; Sun, J.; Qin, F.; Bao, J.; Goddard, W. A.; Chen, S.; Ren, Z. High-performance bifunctional porous non-noble metal phosphide catalyst for overall water splitting. *Nat. Commun.* **2018**, *9* (1), 2551.

(7) Li, A. Y.; Segalla, A.; Li, C.-J.; Moores, A. Mechanochemical Metal-Free Transfer Hydrogenation of Carbonyls Using Polymethylhydrosiloxane as the Hydrogen Source. *ACS Sustainable Chemistry & Engineering* **2017**, *5* (12), 11752−11760.

(8) O'Neill, R. T.; Boulatov, R. The many flavours of mechanochemistry and its plausible conceptual underpinnings. *Nature Reviews Chemistry* **2021**, *5* (3), 148−167.

(9) Chen, Y.; Mellot, G.; van Luijk, D.; Creton, C.; Sijbesma, R. P. Mechanochemical tools for polymer materials. *Chem. Soc. Rev.* **2021**, *50* (6), 4100−4140.

(10) Bhuiyan, F. H.; Li, Y.-S.; Kim, S. H.; Martini, A. Shear-activation of mechanochemical reactions through molecular deformation. *Sci. Rep.* **2024**, *14* (1), 2992.

(11) Humphry-Baker, S. A.; Garroni, S.; Delogu, F.; Schuh, C. A. Melt-driven mechanochemical phase transformations in moderately exothermic powder mixtures. *Nat. Mater.* **2016**, *15* (12), 1280−1286.

(12) Davis, D. A.; Hamilton, A.; Yang, J.; Cremar, L. D.; Van Gough, D.; Potisek, S. L.; Ong, M. T.; Braun, P. V.; Martínez, T. J.; White, S. R.; Moore, J. S.; Sottos, N. R. Force-induced activation of covalent bonds in mechanoresponsive polymeric materials. *Nature* **2009**, *459* (7243), 68−72.

(13) Wu, D.; Lenhardt, J. M.; Black, A. L.; Akhremitchev, B. B.; Craig, S. L. Molecular Stress Relief through a Force-Induced Irreversible Extension in Polymer Contour Length. *J. Am. Chem. Soc.* **2010**, *132* (45), 15936−15938.

(14) Suslick, K. S. Mechanochemistry and sonochemistry: concluding remarks. *Faraday Discuss.* **2014**, *170* (0), 411−422.

(15) Li, S.; Liu, J.; Wang, Z. L.; Wei, D. Mechano-driven chemical reactions. *Green Energy Environ.* **2024**.

(16) Feng, Y.; Ling, L.; Wang, Y.; Xu, Z.; Cao, F.; Li, H.; Bian, Z. Engineering spherical lead zirconate titanate to explore the essence of piezo-catalysis. *Nano Energy* **2017**, *40*, 481−486.

(17) Li, T.; Hu, W.; Tang, C.; Zhou, Z.; Wang, Z.; Shu, L. Enhanced piezo-catalysis in ZnO rods with built-in nanopores. *Journal of Advanced Ceramics* **2023**, *12* (12), 2271−2283.

(18) Schumacher, C.; Hernández, J. G.; Bolm, C. Electro-Mechanochemical Atom Transfer Radical Cyclizations using Piezoelectric BaTiO3. *Angew. Chem., Int. Ed.* **2020**, *59* (38), 16357−16360.

(19) Pang, Y.; Lee, J. W.; Kubota, K.; Ito, H. Solid-State Radical C−H Trifluoromethylation Reactions Using Ball Milling and Piezoelectric Materials. *Angew. Chem., Int. Ed.* **2020**, *59* (50), 22570−22576.

(20) Kubota, K.; Pang, Y.; Miura, A.; Ito, H. Redox reactions of small organic molecules using ball milling and piezoelectric materials. *Science* **2019**, *366* (6472), 1500−1504.

(21) Kimura, M.; Ando, A.; Maurya, D.; Priya, S. Chapter 2 - Lead Zirconate Titanate-Based Piezoceramics. In *Advanced Piezoelectric Materials*, 2 ed; Uchino, K. Ed.; Woodhead Publishing, 2017; pp. 95−126.

(22) Zhang, T. Y.; Gao, C. F. Fracture behaviors of piezoelectric materials. *Theoretical and Applied Fracture Mechanics* **2004**, *41* (1), 339−379.

(23) Anandakrishnan, S. S.; Tabeshfar, M.; Nelo, M.; Peräntie, J.; Jantunen, H.; Juuti, J.; Bai, Y. Recycling hazardous and energy-demanding piezoelectric ceramics using an oxide−halide perovskite upside-down composite method. *RSC Sustainability* **2024**, *2* (4), 961−974.

(24) Xu, S.; Qian, W.; Zhang, D.; Zhao, X.; Zhang, X.; Li, C.; Bowen, C. R.; Yang, Y. A coupled photo-piezo-catalytic effect in a BST-PDMS porous foam for enhanced dye wastewater degradation. *Nano Energy* **2020**, *77*, No. 105305.

(25) Wang, Z. L.; Wang, A. C. On the origin of contact-electrification. *Mater. Today* **2019**, *30*, 34−51.

(26) Wei, Y.; Li, X.; Yang, Z.; Shao, J.; Wang, Z. L.; Wei, D. Contact electrification at the solid−liquid transition interface. *Mater. Today* **2024**, *74*, 2−11.

(27) Galembeck, F.; Burgo, T. A. L.; Balestrin, L. B. S.; Gouveia, R. F.; Silva, C. A.; Galembeck, A. Friction, tribochemistry and triboelectricity: recent progress and perspectives. *RSC Advances* **2014**, *4* (109), 64280−64298.

(28) Du, X.; Huang, J.; Zhang, J.; Yan, Y.; Wu, C.; Hu, Y.; Yan, C.; Lei, T.; Chen, W.; Fan, C.; Xiong, J. Modulating Electronic Structures of Inorganic Nanomaterials for Efficient Electrocatalytic Water Splitting. *Angew. Chem., Int. Ed.* **2019**, *58* (14), 4484−4502.

(29) Fan, F. R.; Tang, W.; Wang, Z. L. Flexible Nanogenerators for Energy Harvesting and Self-Powered Electronics. *Adv. Mater.* **2016**, *28* (22), 4283−4305.

(30) Tang, W.; Jiang, T.; Fan, F. R.; Yu, A. F.; Zhang, C.; Cao, X.; Wang, Z. L. Liquid-Metal Electrode for High-Performance Triboelectric Nanogenerator at an Instantaneous Energy Conversion Efficiency of 70.6%. *Adv. Funct. Mater.* **2015**, *25* (24), 3718−3725.

(31) Wang, Z.; Berbille, A.; Feng, Y.; Li, S.; Zhu, L.; Tang, W.; Wang, Z. L. Contact-electro-catalysis for the degradation of organic pollutants using pristine dielectric powders. *Nat. Commun.* **2022**, *13* (1), 130.

(32) Su, Y.; Berbille, A.; Wang, Z. L.; Tang, W. Water-solid contact electrification and catalysis adjusted by surface functional groups. *Nano Res.* **2024**, *17* (4), 3344−3351.

(33) Zhao, J.; Zhang, X.; Xu, J.; Tang, W.; Lin Wang, Z.; Ru Fan, F. Contact-electro-catalysis for Direct Synthesis of H2O2 under Ambient Conditions. *Angew. Chem., Int. Ed.* **2023**, *62* (21), No. e202300604.

(34) Li, H.; Berbille, A.; Zhao, X.; Wang, Z.; Tang, W.; Wang, Z. L. A contact-electro-catalytic cathode recycling method for spent lithium-ion batteries. *Nat. Energy* **2023**, *8* (10), 1137−1144.

(35) Li, S.; Zhang, Z.; Peng, P.; Li, X.; Wang, Z. L.; Wei, D. A green approach to induce and steer chemical reactions using inert solid dielectrics. *Nano Energy* **2024**, *122*, No. 109286.

(36) Lin, S.; Xu, L.; Chi Wang, A.; Wang, Z. L. Quantifying electron-transfer in liquid-solid contact electrification and the formation of electric double-layer. *Nat. Commun.* **2020**, *11* (1), 399.

(37) Chen, X.; Xia, Y.; Zhang, Z.; Hua, L.; Jia, X.; Wang, F.; Zare, R. N. Hydrocarbon Degradation by Contact with Anoxic Water Microdroplets. *J. Am. Chem. Soc.* **2023**, *145* (39), 21538−21545.

(38) Piradashvili, K.; Alexandrino, E. M.; Wurm, F. R.; Landfester, K. Reactions and Polymerizations at the Liquid−Liquid Interface. *Chem. Rev.* **2016**, *116* (4), 2141−2169.

(39) Li, X.; Li, S.; Guo, X.; Shao, J.; Wang, Z. L.; Wei, D. Triboiontronics for efficient energy and information flow. *Matter* **2023**, *6* (11), 3912−3926.

(40) Jirka, G. P.; Martin, A. F.; Nieman, T. A. pH and concentration response surfaces for the luminol—H2O2 electrogenerated chemiluminescence reaction. *Anal. Chim. Acta* **1993**, *284* (2), 345−349.

https://doi.org/10.1021/jacs.4c09318
J. Am. Chem. Soc. 2024, 146, 31574−31584

(41) Li, M.; Yu, Y.; Li, S.; Wang, F.; Hong, S.; Sun, Y.; Fan, A. A simple chemiluminescent method for the quantification of exosomes based on horseradish peroxidase adsorbed on two-dimensional nanomaterials. *Talanta* **2024**, *275*, No. 126156.
(42) Nakamura, M.; Nakamura, S. One- and Two-Electron Oxidations of Luminol by Peroxidase Systems. *Free Radical Biol. Med.* **1998**, *24* (4), 537−544.
(43) Wang, Z.; An, J.; Nie, J.; Luo, J.; Shao, J.; Jiang, T.; Chen, B.; Tang, W.; Wang, Z. L. A Self-Powered Angle Sensor at Nanoradian-Resolution for Robotic Arms and Personalized Medicare. *Adv. Mater.* **2020**, *32* (32), No. 2001466.
(44) Lin, S.; Zhu, L.; Tang, Z.; Wang, Z. L. Spin-selected electron transfer in liquid−solid contact electrification. *Nat. Commun.* **2022**, *13* (1), 5230.
(45) Fatti, G.; Kim, H.; Sohn, C.; Park, M.; Lim, Y.-w.; Li, Z.; Park, K.-I.; Szlufarska, I.; Ko, H.; Jeong, C. K.; Cho, S. B. Uncertainty and Irreproducibility of Triboelectricity Based on Interface Mechano-chemistry. *Phys. Rev. Lett.* **2023**, *131* (16), No. 166201.
(46) Zhan, F.; Wang, A. C.; Xu, L.; Lin, S.; Shao, J.; Chen, X.; Wang, Z. L. Electron Transfer as a Liquid Droplet Contacting a Polymer Surface. *ACS Nano* **2020**, *14* (12), 17565−17573.
(47) Lu, T.; Chen, F. Multiwfn: A multifunctional wavefunction analyzer. *J. Comput. Chem.* **2012**, *33* (5), 580−592.
(48) Yasui, K. Bubble Dynamics. In *Acoustic Cavitation and Bubble Dynamics*, Yasui, K. Ed.; Springer International Publishing, 2018; pp. 37−97.
(49) Du, Y.; Fu, S.; Shan, C.; Wu, H.; He, W.; Wang, J.; Guo, H.; Li, G.; Wang, Z.; Hu, C. A Novel Design Based on Mechanical Time-Delay Switch and Charge Space Accumulation for High Output Performance Direct-Current Triboelectric Nanogenerator. *Adv. Funct. Mater.* **2022**, *32* (48), No. 2208783.
(50) Li, S.; Zhang, Z.; Yang, F.; Li, X.; Peng, P.; Du, Y.; Zeng, Q.; Willatzen, M.; Wang, Z. L.; Wei, D. Transistor-like triboiontronics with record-high charge density for self-powered sensors and neurologic analogs. *Device* **2024**, *2*, No. 100332.
(51) Lin, S.; Chen, X.; Wang, Z. L. Contact Electrification at the Liquid−Solid Interface. *Chem. Rev.* **2022**, *122* (5), 5209−5232.
(52) Okouchi, S.; Nojima, O.; Arai, T. Cavitation-Induced Degradation of Phenol by Ultrasound. *Water Sci. Technol.* **1992**, *26* (9−11), 2053−2056.
(53) Mahvi, A. H.; Maleki, A. Photosonochemical degradation of phenol in water. *Desalination and Water Treatment* **2010**, *20* (1−3), 197−202.
(54) Wu, C.; Liu, X.; Wei, D.; Fan, J.; Wang, L. Photosonochemical degradation of Phenol in water. *Water Res.* **2001**, *35* (16), 3927−3933.
(55) Maleki, A.; Mahvi, A. H.; Mesdaghinia, A.; Naddafi, K. Degradation and toxicity reduction of phenol by ultrasound waves. *Bulletin of the chemical society of Ethiopia* **2007**, *21* (1), DOI: .
(56) Lv, W.; Kong, L.; Lan, S.; Feng, J.; Xiong, Y.; Tian, S. Enhancement effect in the piezoelectric degradation of organic pollutants by piezo-Fenton process. *J. Chem. Technol. Biotechnol.* **2017**, *92* (1), 152−156.
(57) Thangavel, S.; Pazhamalai, P.; Krishnamoorthy, K.; Sivalingam, Y.; Arulappan, D.; Mohan, V.; Kim, S.-J.; Venugopal, G. Ferroelectric-semiconductor BaTiO3−Ag2O nanohybrid as an efficient piezo-photocatalytic material. *Chemosphere* **2022**, *292*, No. 133398.
(58) Zheng, H.; Chen, J.; Que, M.; Yang, T.; Liu, Z.; Cai, W.; Yang, L.; Liu, X.; Li, Y.; Yang, X.; Ma, Y.; Zhu, G. Highly efficient piezoelectric field enhanced photocatalytic performance via in situ formation of BaTiO3 on Ti3C2Tx for phenolic compound degradation. *Inorganic Chemistry Frontiers* **2022**, *9* (16), 4201−4215.
(59) Brown, M. A.; Goel, A.; Abbas, Z. Effect of Electrolyte Concentration on the Stern Layer Thickness at a Charged Interface. *Angew. Chem., Int. Ed.* **2016**, *55* (11), 3790−3794.
(60) Gillespie, R. J. The VSEPR model revisited. *Chem. Soc. Rev.* **1992**, *21* (1), 59−69.
(61) Hurley, A. C.; Lennard-Jones, J. E.; Pople, J. A. The molecular orbital theory of chemical valency XVI. A theory of paired-electrons in polyatomic molecules. *Proc. R. Soc. Lond. Ser. A. Math. Phys. Sci.* **1997**, *220* (1143), 446−455.
(62) Chirgwin, B. H.; Coulson, C. A.; Randall, J. T. The electronic structure of conjugated systems. VI. *Proc. R. Soc. Lond. Ser. A. Math. Phys. Sci.* **1997**, *201* (1065), 196−209.
(63) Steele, D.; Quatermain, A. The vibrational spectra of amides—II. The force field and isotopic shifts of N,N-dimethyl formamide. *Spectrochimica Acta Part A: Molecular Spectroscopy* **1987**, *43* (6), 781−789.
(64) Decker, H. Ueber die Beziehungen des doppelt gebundenen Kohlenstoffs zum Stickstoff, Sauerstoff und Schwefel. *Berichte der deutschen chemischen Gesellschaft* **1905**, *38* (3), 2493−2511.
(65) Bard, A. J.; Faulkner, L. R.; White, H. S. *Electrochemical methods: fundamentals and applications*; John Wiley & Sons, 2022.
(66) Yen, A. S.; Kim, S. S.; Hecht, M. H.; Frant, M. S.; Murray, B. Evidence That the Reactivity of the Martian Soil Is Due to Superoxide Ions. *Science* **2000**, *289* (5486), 1909−1912.
(67) Zhang, J.; Liu, J. Nanozyme-based luminescence detection. *Luminescence* **2020**, *35* (8), 1185−1194.
(68) Jia, L.; Xu, J.-P.; Li, D.; Pang, S.-P.; Fang, Y.; Song, Z.-G.; Ji, J. Fluorescence detection of alkaline phosphatase activity with β-cyclodextrin-modified quantum dots. *Chem. Commun.* **2010**, *46* (38), 7166−7168.
(69) Tong, Y.-J.; Song, A.-M.; Yu, L.-D.; Liang, R.-P.; Qiu, J.-D. Aggregation-induced fluorescence of the luminol-terbium(III) complex in polymer nanoparticles for sensitive determination of thrombin. *Microchim. Acta* **2019**, *187* (1), 53.
(70) Barni, F.; Lewis, S. W.; Berti, A.; Miskelly, G. M.; Lago, G. Forensic application of the luminol reaction as a presumptive test for latent blood detection. *Talanta* **2007**, *72* (3), 896−913.
(71) Hyland, K.; Auclair, C. The formation of superoxide radical anions by a reaction between O2, OH−and dimethyl sulfoxide. *Biochem. Biophys. Res. Commun.* **1981**, *102* (1), 531−537.
(72) Gorsuch, J. D.; Hercules, D. M. Studies on the Chemiluminescence of Luminol in Dimethylsulfoxide and Dimethylsulfoxide-Water Mixtures. *Photochem. Photobiol.* **1972**, *15* (6), 567−583.
(73) Shi, M.-J.; Cui, H. Electrochemiluminescence of luminol in dimethyl sulfoxide at a polycrystalline gold electrode. *Electrochim. Acta* **2006**, *52* (3), 1390−1397.

https://doi.org/10.1021/jacs.4c09318
J. Am. Chem. Soc. 2024, 146, 31574−31584